BIOCHEMISTRY
including biophysical chemistry & molecular biology

Article

pubs.acs.org/biochemistry

Unique Residues at the 3-Fold and 4-Fold Axis of Mycobacterial Ferritin Are Involved in Oligomer Switching

Garima Khare, Prachi Nangpal, and Anil K. Tyagi*

Department of Biochemistry, University of Delhi South Campus, Benito Juarez Road, New Delhi 110021, India

Supporting Information

ABSTRACT: To identify the crucial residues involved in the self-assembly and function of BfrB, one of the important iron storage proteins of *Mycobacterium tuberculosis*, we constructed various mutants by employing site-directed mutagenesis. The analysis of mutants led to the identification of "interface hot-spot residues" (R69, L129, and F159) that act as "switch points" for BfrB oligomerization, and our observations show the importance of 4-fold axis residues in assembly formation. Moreover, we demonstrate that single-point mutations Q51A, Q126A, and E135A can enhance the thermal stability of the protein without affecting its assembly. Importantly, a comparative analysis of various mutations revealed that the function of various homologous positions in different ferritins could be at variance; hence, predicting the function of a residue just based on sequence−structure comparisons may not be appropriate. Thus, we report the identification of novel residues in the assembly formation and function of BfrB and show that single-point mutations have a remarkable potential for alteration of multiple properties of ferritins. Besides, "switch residues" or "interface hot spots" identified in this study could also prove to be helpful for the rational design of interfacial inhibitors.

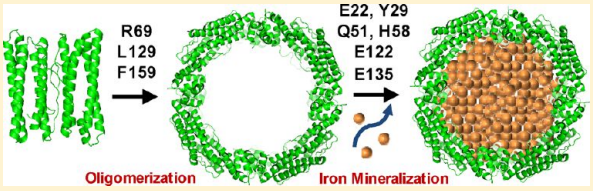

Ferritins are macromolecular spherical structures with a cagelike cavity in which they sequester iron in mineralized form and play an important role in maintaining iron homeostasis.[1−5] Ferritin upregulation has been reported in a number of autoimmune disorders such as lupus and rheumatoid arthritis.[6,7] It has been demonstrated in a number of organisms, including *Mycobacterium tuberculosis* that ferritins are upregulated under iron excessive conditions, where they store the excess iron in their cavity and prevent the cells from being subjected to iron toxicity.[8,9] Recently, our laboratory has shown that the disruption of bacterioferritins leads to a marked attenuation of the disease causing ability of the pathogen in animal models.[10] Hence, because of their pivotal role in iron homeostasis, ferritins have also been proposed as potential drug targets against many disease-causing pathogens.[10,11]

Three classes of ferritins exist: the non-heme binding ferritins, heme binding bacterioferritins, and DNA binding proteins from starved cells termed Dps.[12] Ferritin molecules exhibit a general quaternary structure of 24 subunits assembled into an octahedral 432 symmetric arrangement to form spherical shells enclosing a hollow cavity that has the ability to hold up to ∼5000 iron atoms.[13−15] Formation of iron mineral at the ferritin cavity involves a complex series of events. The cascade of events leading to iron storage under an excess of iron involves binding of ferrous iron to ferritin protein and its migration to the ferroxidase catalytic center by means of various channels and pores wherein ferrous iron Fe(II) is oxidized to the ferric Fe(III) state. Subsequently, Fe(III) is transferred and sequestered as ferric mineral in the storage cavity of ferritin, which can be made available for the cell at the time of iron deprivation. A significant number of studies have been devoted to the identification of residues involved in various stages of iron storage.[16−25] Primarily, there are three main aspects of the mechanism of ferritins that have been the focus of most of the mutagenic studies. The first is the identification of residues involved in the ferroxidase activity of the protein. Evidence of the involvement of a few conserved glutamate residues located at the ferroxidase center in iron oxidation has been shown by many structural and mutagenesis studies.[16,17] Besides, substitutions of conserved residues E62 and H65 in human H-chain ferritin have also been shown to eliminate the binding of Fe(II) to the ferroxidase center.[18] The second area is the identification of regions contributing to the entry and exit of iron. A growing body of evidence indicates that the 3-fold pore or channel constitutes the iron entry site.[19,20] In addition, in a study of recombinant frog H-ferritin, Theil and co-workers have demonstrated that substitution of the leucine residue at position 134 with proline (L134P) lying at the 3-fold channel led to a marked increase in the rate of iron release, a phenomenon explained by localized unfolding at this site, suggesting that the interactions leading to the proper structure of the 3-fold channel are required for regulated iron release as well.[21,22] However, the involvement of the 3-fold channel in iron exit is limited to these few studies on this particular residue. Besides, a few studies also speculate about the role of 4-fold channels in the release of iron.[23] The third area of investigation, although not explored in great detail, is related to the formation and stability of assembly of ferritins. The simultaneous substitution of two glutamate residues in the 3-

Received: September 3, 2012
Revised: February 8, 2013
Published: February 14, 2013

dx.doi.org/10.1021/bi301189t | *Biochemistry* 2013, 52, 1694−1704

fold channel of *Rhodobacter capsulatum* bacterioferritin has been shown to render the protein incapable of assembling into a 24-mer.[24] Also, the mutation of a few residues from the 3-fold channel that are involved in subunit interactions are reported to result in the formation of stable subunit dimers of *Escherichia coli* bacterioferritin rather than 24-meric assembly.[25] Although there has been enough emphasis on understanding the iron uptake and ferroxidase activity, there are not enough studies to clearly demonstrate the role of 3-fold and 4-fold channel residues in assembly formation of these cagelike proteins.

Recently, we reported the crystal structure of bacterioferritin B (BfrB) of *M. tuberculosis*, and its comparative analysis with the representatives of the ferritin families belonging to the archaea, eubacteria, and eukarya identified the slowly evolving conserved sites as well as the rapidly evolving variable sites and analyzed the role of a unique and extended C-terminus in relation to the structure and function of the protein.[26] Herein, we have employed site-directed mutagenesis to identify residues important for interactions between subunits of this ferritin that are required for molecular assembly, structural integrity, thermodynamic stability, and ferroxidase activity to provide an improved understanding of the determinants of self-assembly and the structure−function relationship.

MATERIALS AND METHODS

Cloning and Expression of *M. tuberculosis bfrB* and Generation of Mutants. The *bfrB* gene (*rv3841*), previously cloned in pET21c,[26] was excised from it and subcloned in pASK-iba43+ at *Nhe*I and *Hin*dIII sites. For the generation of various *bfrB* mutants, the XL-GOLD Quick Change kit was employed (Stratagene, La Jolla, CA). The primers used for generating the mutations are listed in Table 1. Polymerase chain reaction amplification of pASK-iba43+ carrying the wild-type *bfrB* gene (pASK-iba43+*bfrB*) was conducted by using the primers designed for mutagenesis followed by *Dpn*I digestion. *E. coli* XL-1Blue cells were transformed with the reaction mixture. The mutations were confirmed by DNA sequencing. *E. coli* BL21(λDE3) cells were transformed either with pASK-iba43+*bfrB* or with pASK-iba43+ carrying the mutated versions of the gene. Transformed cells were grown in Luria-Bertani medium containing 50 μg/mL ampicillin at 37 °C to an A_{600} of 0.8−1.0 followed by induction with anhydrotetracycline at a concentration of 200 ng/mL for 3 h at 37 °C with the exception of mutant E22A, which was induced at 18 °C for 16 h because of the limited solubility of the protein product. The overexpressed protein was localized in the soluble fraction of the cell [20 kDa band (Figure S1 of the Supporting Information, lane 5)] and was subjected to purification.

Table 1. Oligonucleotides Used for Generating Site-Directed Mutants of BfrB

mutation	mutagenic oligonucleotide[a]
E22A (F)	5′-ggaacagattcataac**gca**ttcacagcggcac-3′
E22A (R)	5′-gtgccgctgtgaa**tgc**gttatgaatctgttcc-3′
Y29A (F)	5′-cacagcggcacaacaa**gcg**gtcgcgatcgcgg-3′
Y29A (R)	5′-ccgcgatcgcgac**cgc**ttgttgtgccgctgtg-3′
Q51A (F)	5′-gcatttttacagc**gca**gcggtcgaggaacg-3′
Q51A (R)	5′-cgttcctcgaccgc**tgc**gctgtaaaaatgc-3′
H58A (F)	5′-gtcgaggaacgaaac**gcg**gcaatgatgctcgtg-3′
H58A (R)	5′-cacgagcatcattgc**cgc**gtttcgttcctcgac-3′
R69A (F)	5′-caacacctgctcgac**gcc**gaccttcgtgtc-3′
R69A (R)	5′-gacacgaaggtc**ggc**gtcgagcaggtgttg-3′
E122A (F)	5′-gcgatttcctcggc**gcg**cagttcatgcagtg-3′
E122A (R)	5′-cactgcatgaactg**cgc**gccgaggaaatcgc-3′
Q126A (F)	5′-cggcgagcagttcatg**gcg**tggttcttgcagg-3′
Q126A (R)	5′-cctgcaagaacca**cgc**catgaactgctcgccg-3′
W127A (F)	5′-gcagttcatgca**ggcg**ttcttgcaggaac-3′
W127A (R)	5′-gttcctgcaagaa**cgc**ctgcatgaactgc-3′
L129P (F)	5′-gttcatgcagtggttc**ccg**caggaacagatcg-3′
L129P (R)	5′-cgatctgttcctg**cggg**aaccactgcatgaac-3′
E135A (F)	5′-gcaggaacagatcgaa**gcg**gtggccttgatgg-3′
E135A (R)	5′-ccatcaaggccacc**gc**ttcgatctgttcctgc-3′
F159A (F)	5′-gttcgagctagagaac**gcc**gtcgcacgtgaag-3′
F159A (R)	5′-cttcacgtgcgac**ggc**gttctctagctcgaac-3′
E157A/F159A (F)	5′-ccaacctgttcgagcta**gcg**aac**gcc**gtcgcacgtgaagtg-3′
E157A/F159A (R)	5′-cacttcacgtgcgac**ggc**gtt**cgc**tagctcgaacaggttgg-3′

[a]Mutagenic regions are bold.

Preparation of the Cell Free Extract. After induction of the cultures, the cells were harvested by centrifugation and resuspended in 20 mM Tris-HCl (pH 8.0) containing 50 mM NaCl, 2 mM β-mercaptoethanol, and 1 mM phenylmethanesulfonyl fluoride. Cells were disrupted with a French press followed by centrifugation at 16000*g* for 45 min. From the cell free lysate obtained after centrifugation, the 24-meric assembled form and subunit dimeric form of BfrB were purified as described below.

Purification of the 24-meric Assembled Form. The cell lysate was subjected to 0 to 25% ammonium sulfate precipitation followed by centrifugation at 13000*g* for 1 h at 4 °C. A Sephacryl S-300 column (2.5 cm × 100 cm, exclusion range of 10−1500 kDa) pre-equilibrated with 20 mM Tris-HCl (pH 8.0) containing 100 mM NaCl (buffer A) was loaded with the 0 to 25% ammonium sulfate precipitate suspended in 5 mL of buffer A, developed at a flow rate of 0.5 mL/min, and 5 mL fractions were collected. In the case of the wild-type protein and most of the mutants (E22A, Y29A, Q51A, H58A, E122A, Q126A, W127A, and E135A), a majority of the protein eluted as a 24-meric assembled species (480 kDa, elution volume of 250 mL) and a small fraction eluted as a disassembled subunit dimeric form (40 kDa, elution volume of 320 mL). The peak representing the 24-meric assembled form was collected and used for further studies. Molecular masses of the proteins were calculated on the basis of the elution volumes of standard protein markers. The proteins were analyzed for purity by sodium dodecyl sulfate−polyacrylamide gel electrophoresis (SDS−PAGE) on a 12.5% gel. The protein concentration was determined by using Bradford's reagent with bovine serum albumin as the standard.

Purification of the Subunit Dimeric Form. The subunit dimeric form of BfrB mutants R69A, L129P, F159A, and E157A/F159A was also purified by employing ammonium sulfate precipitation and gel filtration chromatography. For this, the cell free lysate was subjected to 0 to 25% ammonium sulfate precipitation followed by suspension of the precipitate in buffer A, which was then loaded onto a Sephacryl S-300 column (2.5 cm × 100 cm, exclusion range of 10−1500 kDa). The column was developed at a rate of 0.5 mL/min with buffer A, and the 5 mL fractions were collected. Analysis of the fractions revealed that the subunit dimer was eluted as a single peak at 320 mL (corresponding to 40 kDa) and no peak was observed in place of the 24-meric assembled protein. Molecular masses of the proteins were calculated on the basis of the elution volumes of the standard protein markers.

dx.doi.org/10.1021/bi301189t | *Biochemistry* 2013, 52, 1694−1704

Analytical Gel Filtration Chromatography. The subunit composition of wild-type BfrB and its mutants was determined by size exclusion chromatography (SEC) employing a 3 mL Superdex G-200 column (5 mm × 150 mm) with an exclusion range of 10−600 kDa (pre-equilibrated with buffer A) on an AKTA 10 FPLC purifier (GE Healthcare Bio-Sciences AB, Uppsala, Sweden). Protein samples were loaded onto the column, and the absorbance of the eluted fractions was measured at 280 nm. The molecular mass and the oligomerization status of the proteins were calculated by using the standard protein markers.

Transmission Electron Microscopy (TEM). Proteins at a concentration of 1 mg/mL were fixed by using the "single-droplet" parafilm protocol. The protein sample was overlaid onto a 300-mesh carbon/Formvar-coated grid and allowed to absorb to the Formvar for a minimum of 1 min. Excess fluid was removed by using filter paper, and the grid was dipped in saturated solution of uranyl acetate for an additional 1 min. Finally, the grids were dried and placed into the grid chamber, and samples were observed with a JEOL JEM-200F transmission electron microscope (at the Advanced Instrumentation Research Facility, Jawaharlal Nehru University, Delhi, India). For visualization of the stored iron cores, the purified protein was converted into holoferritin by incubating a 0.25 μM protein solution with 125 μM ammonium ferrous sulfate (freshly prepared in 0.015 N HCl) in 0.1 M HEPES (pH 6.5) for 2 h at room temperature. Free or unbound iron, if any, was removed by passing the sample through a Microcon centrifugal filter device (Millipore Corp.) with a 10 kDa membrane. The sample was then overlaid onto a 300-mesh carbon/Formvar-coated grid and allowed to absorb to the Formvar for a minimum of 1 min and subsequently visualized in the electron microscope.

Circular Dichroism Spectroscopy. Far-UV CD spectra were recorded on a J-815 spectropolarimeter (JASCO Corp., Hachioji-shi, Tokyo, Japan). An average of three scans was taken, and the spectra were obtained at an interval of 0.1 nm with a scanning speed of 50 nm/min using a 1 mm path length quartz cuvette. A protein concentration of 0.05 mg/mL in 10 mM sodium phosphate (pH 8.0) was employed. For thermal denaturation studies, spectra were recorded at various temperatures maintained through an attached water bath with a 5 min incubation at the desired temperature.

Kinetic Measurements of Iron Oxidation. To a 0.25 μM protein solution was added 125 μM ammonium ferrous sulfate freshly prepared in 0.015 N HCl and 0.1 M HEPES (pH 6.5). The iron oxidation was monitored by an increase in the optical density at 310 nm, which specifically measures Fe(III) ions, and the kinetic measurements were recorded from the time of addition of iron to the protein. The subunit dimeric mutants R69A, L129P, F159A, and E157A/F159A were not employed for functional studies because of the lack of functional ferritin shells in these mutants.

Iron Incorporation by Prussian Blue Staining. Twenty micrograms of each protein was incubated with 0.5 mM ammonium ferrous sulfate freshly prepared in 0.015 N HCl in 0.1 M HEPES (pH 6.5) in a reaction volume of 40 μL. The reaction mix was incubated for 2 h at room temperature allowing Fe(II) oxidation and subsequently incorporation as Fe(III) ions in the protein shell. Further, the reaction mix was separated by native PAGE on a 7.5% gel and stained with Coomassie Brilliant Blue (protein staining) and Prussian blue (iron staining). Prussian blue (2% potassium ferrocyanide in 10% HCl) specifically forms a blue coordination complex with Fe(III) ions. The gel was incubated with Prussian blue stain for 5−10 min followed by removal of the excessive stain by washing with water.

RESULTS

Influence of Various Mutations on the Molecular Assembly of BfrB Nanocage Protein. Twelve site-directed mutants were generated by using the appropriate oligonucleotides (Table 1 and Figure 1). The residues were chosen on the basis of the three-dimensional structure of mycobacterial BfrB reported previously by us.[26] The proteins were purified to homogeneity by using a two-step protocol as described in Materials and Methods, analyzed by SDS−PAGE on a 12.5% gel, and found to be homogeneously pure. The result of purification of wild-type BfrB is shown in Figure S2 of the Supporting Information. In addition, it was found that the yield of BfrB was ∼120 mg/L of culture, and we emphasize that we have developed a very efficient system for high-yield expression of this nanocage ferritin. The monomeric size of a single BfrB subunit is 20 kDa (Figure S2 of the Supporting Information). It was found that in the case of the wild-type protein and most of the mutants (E22A, Y29A, Q51A, H58A, E122A, Q126A, W127A, and E135A), the protein existed primarily as a 24-meric assembled form. However, in the case of mutants R69A, L129P, F159A, and E157A/F159A, we observed that these mutant proteins completely disassembled into subunit dimeric forms.

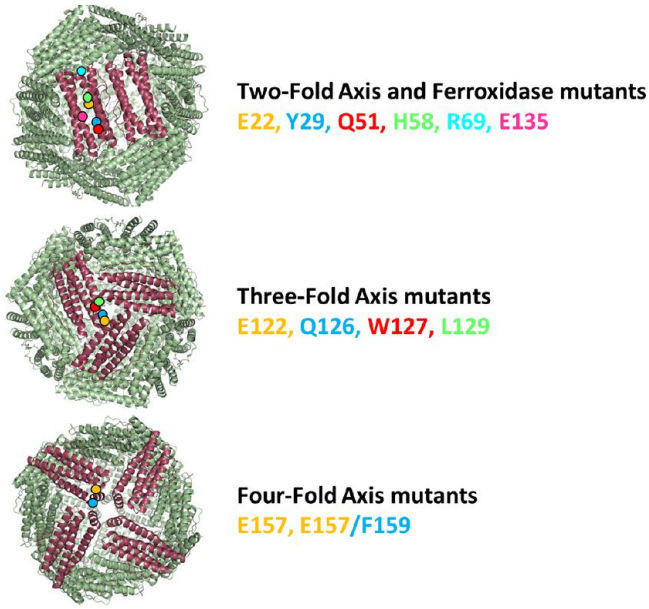

Figure 1. Location of residues selected for site-directed mutagenesis. The ribbon representation of the BfrB structure (green) is shown with 2-, 3-, and 4-fold symmetric axes highlighted (salmon), with the location of the residues chosen for mutagenesis shown as colored dots in one of the highlighted subunits.

The purified BfrB protein and the mutants were further analyzed by electrophoresis on a 7.5% native polyacrylamide gel (Figure 2A). The BfrB WT protein appeared as a mixture of 24-mer and subunit dimer as was evident by the presence of two bands in the native gel; however, the 24-mer was present as the predominant species (82%) (Figure 2A, lane 1, and Figure 2B). This observation is consistent with the literature, wherein the ferritin proteins that were purified as 24-mers often reappeared

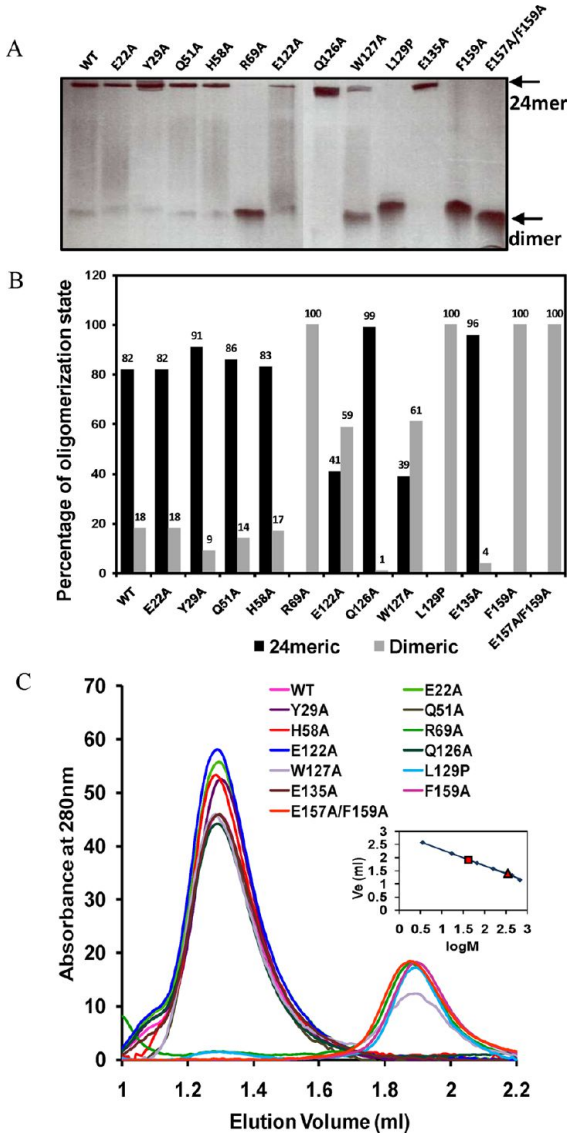

Figure 2. Single-point mutations disrupt the assembly formation of BfrB. (A) Analysis of wild-type (WT) BfrB and its mutants on a 7.5% native polyacrylamide gel. The arrows represent the assembly size of the purified proteins. The knowledge of the molecular size of these bands was derived from the gel filtration data based on the use of molecular mass marker proteins. The purified peaks of the 24-meric assembled form as well as the subunit dimeric form from samples eluted via gel filtration were loaded separately on a native gel. Lanes for mutants R69A, L129P, F159A, and E157A/F159A indicate that these four BfrB mutants exist as subunit dimers in solution, confirming that these amino acids play a key role in the oligomerization of the protein. (B) Bar diagram showing the percentage of the 24-meric form present in WT and all the mutants. (C) Size exclusion chromatographic profile of WT BfrB and its mutants, where the inset shows the standard calibration curve along with a triangle and a square representing the elution volume of the 24-mer and subunit dimer, respectively.

as a mixture of 24-mer and subunit dimer on native gel analysis.[25,27,28] This probably results from protein degradation, although further work would be required to resolve this uncertainty. Further, we evaluated the iron content of this purified protein and observed that the purified protein stained negatively for Prussian blue (Figure S3A of the Supporting Information) and exhibited fewer than two Fe atoms per protein by reductive ferrozine assay[29] and fewer than five Fe atoms per protein by atomic absorption spectroscopy. This negligible amount of iron in the protein thus demonstrated that the purified protein was in the apo form. Hence, the assembly of the protein was not dependent upon iron. Similar observations have also been reported in the case of other ferritins such as bullfrog Ftn, wherein overproduction of this ferritin as a recombinant protein results in the isolation of apoferritin with negligible amount of iron (five or fewer Fe atoms per protein).[20,30] The clinching evidence that ruled out the possibility that protein assembly may depend upon iron was provided when we conducted the reductive chelation of any possible iron present in the protein via the addition of sodium ascorbate and ferrozine reagent, which leads to reduction and sequestration of iron due to formation of a complex between iron and ferrozine. The reaction was monitored for more than 24 h to ensure complete removal of iron. It was observed that in spite of complete sequestration of any possible iron in the protein, the latter still existed in a 24-meric assembly as analyzed by native polyacrylamide gel electrophoresis (Figure S3B of the Supporting Information). Hence, the assembly and disassembly of the protein are not related to its iron content. Mutants R69A, L129P, F159A, and E157A/F159A migrated only as fast running species that corresponded to the subunit dimer in the absence of the higher oligomeric form (Figure 2A,B). These results clearly suggested that residues R69, L129, and F159 are involved in the self-assembly of BfrB and act as "switch residues" for oligomerization. In addition, the predominace of the 24-meric assembled form was found to be reduced in mutants W127A (from 82 to 39%) and E122A (from 82 to 41%) in comparison to the native protein, suggesting the involvement of these residues in providing stability to the assembled form (Figure 2A,B). Interestingly, mutation of residues Q126 and E135 to alanine resulted in a marked increase in the percentage of the 24-meric form (from 82 to ~96−99%), suggesting that these mutations provide a higher stability to the macromolecular form (Figure 2B). The 24-meric assembled forms as well as the subunit dimeric forms of the protein described above were further confirmed by subjecting the purified proteins to FPLC analysis by using a G-200 Superdex column (5 mm × 150 mm, exclusion range of 10−600 kDa), and the molecular masses of the proteins were determined on the basis of the elution volumes of the known standard proteins (Figure 2C).

Analysis of Cage Formation by Transmission Electron Microscopy. Ferritins represent a unique example of protein structures that form nanocages; hence, we next wanted to show that the purified wild-type protein represented functional ferritin shells that can store iron. In addition, we wanted to analyze the influence of mutations on the assembly of the protein that can be visualized in solution by TEM analysis after the proteins had been stained with uranyl acetate. As stated above, mutants R69A, L129P, F159A, and E157A/F159A exhibited altered molecular assemblies and existed as subunit dimers when analyzed by native gel electrophoresis. Their inability to assemble into 24-meric nanocages was further verified by employing TEM. Besides, two mutant proteins, E22A and H58A, which showed no alteration in the molecular assembly as a result of associated mutations, were also included for the sake of comparison (Figure 3). The micrograph images for BfrB showed ~15 nm nanocage structures with a cavity size of ~5 nm. The holoferritin molecules (preincubated with iron) could be visualized without any staining because of the

dx.doi.org/10.1021/bi301189t | *Biochemistry* 2013, 52, 1694−1704

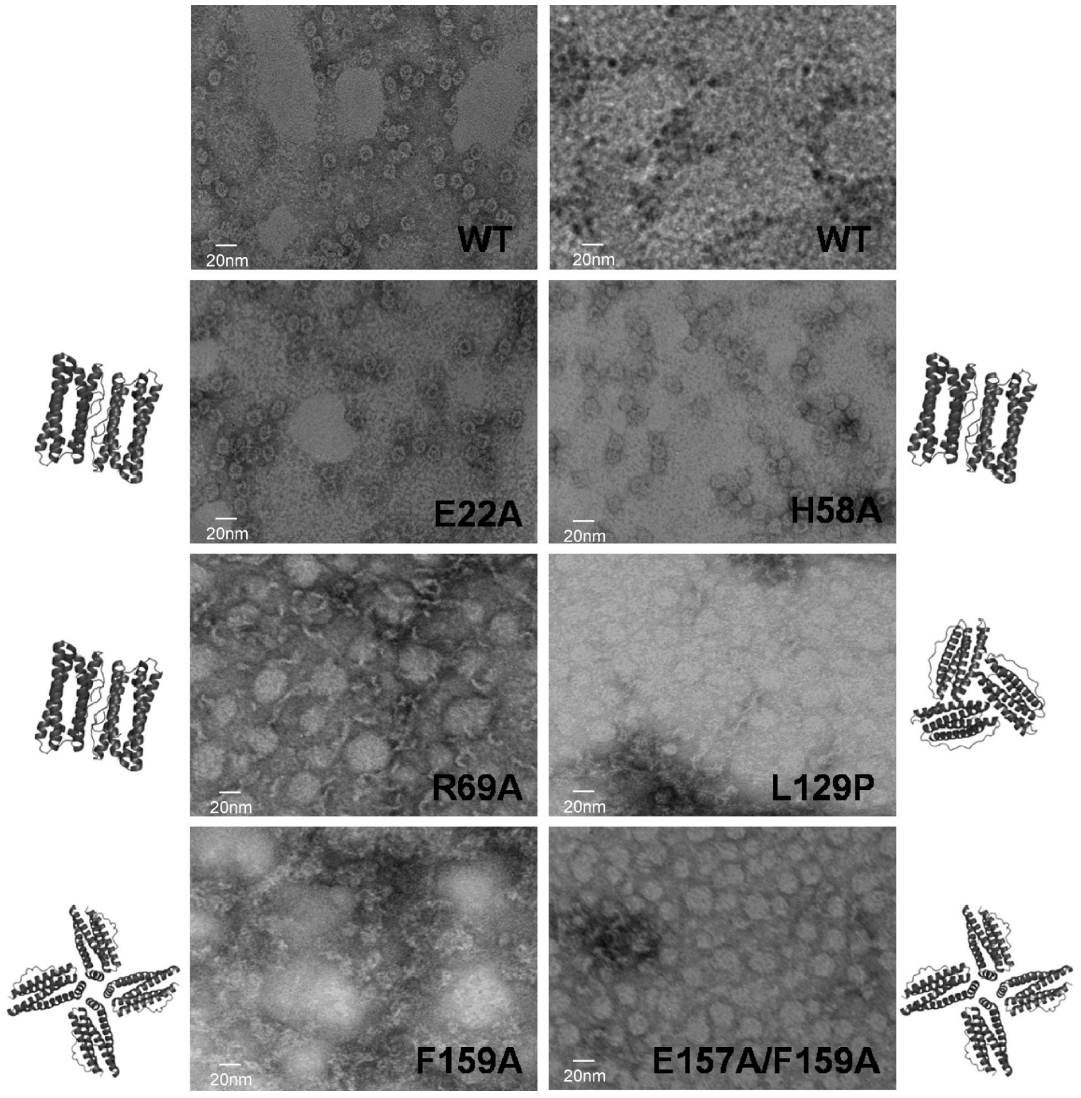

Figure 3. Analysis of nanocage formation by WT BfrB and its mutants by TEM analysis. The topmost TEM micrograph in the left column shows the uranyl acetate-stained sample of WT BfrB showing the presence of nanocage assembly of the protein. The topmost micrograph in the right column shows the unstained sample of WT to depict the stored iron in WT. The other micrographs show the uranyl acetate-stained samples of mutants E22A, H58A, R69A, L129P, F159A, and E157A/F159A. The side panel on both sides of the micrographs indicates the location of the involved mutation in the 2-, 3-, or 4-fold axis. The substitution of residues R69, L129, and F159 resulted in an inability to form nanocages, indicating the essential requirement of these residues for assembly formation.

accumulation of iron marked by intense dark spots (~5 nm) (Figure 3). The top panel in Figure 3 shows the stained (left panel) and unstained (right panel) protein after incubation of the protein with iron in a ratio of 1:500 (protein:iron). Hence, the top left panel shows that the wild-type protein is in the assembled form. The right panel that is not stained does not show the protein structure but shows the presence of iron as dense spots, which are stored inside the protein's cavity. Hence, it verifies that the purified protein is in the functionally assembled form and can be converted to its holo form after incubation with iron. However, the entire ferritin population is not seen to be in the holo form as the iron incubation was performed under nonsaturating conditions. As expected, the mutant proteins with altered assemblies existing as subunit dimeric forms (R69A, L129P, F159A, and E157A/F159A) displayed no formation of nanocages (Figure 3), and no accumulation of iron was exhibited either (data not shown). E22A and H58A, the mutant proteins with normal molecular assembly, showed up as the wild-type BfrB protein (Figure 3). These results substantiate the importance of residues R69, L129, and F159 in the formation of macromolecular nanocage assembly of the protein.

Identification of Residues Markedly Affecting the Secondary Structure and Thermal Stability of BfrB Nanocages. The secondary structure and thermal stability are important determinants of the structural integrity of a protein. It would indeed also be useful to be able to create single-point mutations that can alter the structural properties of the protein as desired. We were thus keen to determine the influence of the mutated residues on the secondary structure and thermal stability, especially for the mutants with altered assemblies. The secondary structure of the proteins was analyzed by circular dichroism. As is evident by the results depicted in Figure 4A, the wild type and the mutant proteins exhibited a well-folded structure with a characteristic pattern of α-helical proteins. Most of the mutants displayed a profile

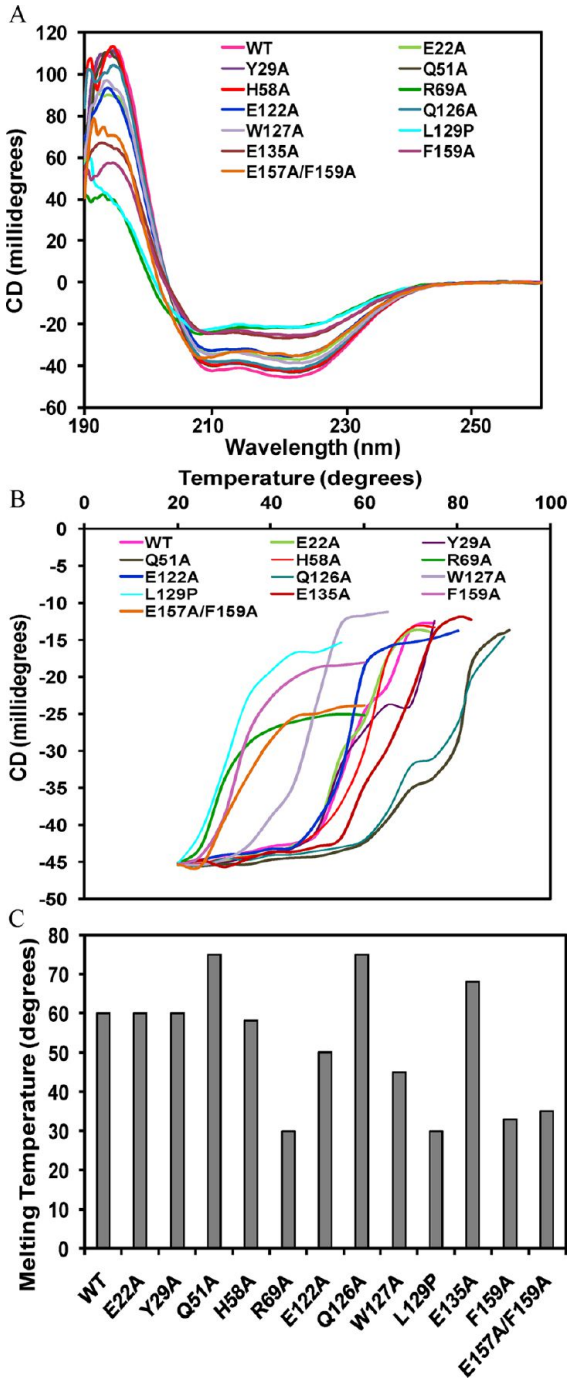

Figure 4. Influence of various mutations on the secondary structure and thermal stability of BfrB. (A) Secondary structure analysis of all the proteins by circular dichroism. (B) Thermal denaturation curves were monitored by measuring CD values at 222 nm with an increase in temperature. (C) Bar diagram depicting the melting temperatures of WT BfrB and its mutants. The subunit dimeric forms of BfrB mutants R69A, L129P, F159A, and E157A/F159A show a reduced melting temperature as compared to those of WT BfrB and other BfrB mutants, suggesting that these residues are involved in important interactions during assembly formation. Two separate experiments were conducted, and one of the representative curves is depicted.

similar to that of the wild-type protein; however, mutants R69A, L129P, and F159A, which existed as subunit dimeric forms, exhibited a reduced secondary structure. Besides, even though mutant E157A/F159A also existed as a subunit dimeric form, the expected reduction in the secondary structure was not observed in this case, and in contrast to R69A, L129P, and F159A mutants, this mutant retained normal secondary structure. Moreover, mutant E135A exhibited no alteration in the assembly of the protein, yet a significant reduction in its secondary structure was observed (Figure 4A).

The thermal stability of all the mutants was compared with that of wild-type BfrB by circular dichroism measurements at 222 nm for the determination of melting temperatures (Figure 4B). Wild-type BfrB exhibited a characteristic sigmoidal pattern of thermal denaturation, suggesting a cooperative unfolding of the assembly wherein the structure remains unaffected by temperature until it reaches 50 °C and exhibited a melting temperature of 60 °C. Mutations at the ferroxidase center (E22A, Y29A, and H58A) exhibited no influence on the thermal stability of the mutants, whereas subunit dimeric mutants (R69A, L129P, F159A, and E157A/F159A) were extremely labile to heat treatment and began to unfold even at ∼30 °C (Figure 4C). In addition, the melting temperatures of mutants W127A and E122A were between the melting temperatures of wild-type BfrB and subunit dimeric mutants. These observations further substantiate the higher percentage of the subunit dimeric form in these mutants as compared to that of the wild type. Most importantly, the mutants related to metal binding (E135 and Q51) and 3-fold channel formation (Q126), which remained perfectly assembled in spite of substitutions, exhibited a significantly higher thermal stability than wild-type BfrB with T_m values in the range of 70−75 °C (Figure 4C). Of these, mutant E135A seems to be of special interest as despite the reduction in the level of secondary structure, it exhibited normal assembly of the protein and, unexpectedly, its thermal stability was significantly enhanced.

Identification of Residues That Influence the Ferroxidase Activity of the Protein. We next evaluated the influence of the targeted residues on the ferroxidase activity of BfrB. The rate of iron oxidation was monitored by measuring the increase in absorbance at 310 nm in the presence of iron (Figure 5A,B and Figures S4 and S5 of the Supporting Information). The pH is known to have a drastic effect on the autoxidation property of iron under specific buffer conditions, which complicates the measurement of protein-mediated oxidation of iron. Hence, before conducting the experiments for the iron oxidation by BfrB and its mutants, we established the optimal pH conditions for this reaction using WT BfrB (Figure S4 of the Supporting Information). As can be analyzed from the iron oxidation curves in Figure S4, pH 6.5 represents the optimal condition for conducting these experiments as iron exhibits the least autoxidation at this pH in comparison to the actual iron oxidation by the protein. However, at lower pH values, the protein-based oxidation itself was much lower, and at higher pH values, the autoxidation rate was significantly high. Figure 5B shows a comparison of the percent difference in the rate of iron oxidation between the wild-type protein and the various mutants. We observed that mutation of residues associated with the ferroxidase activity (E22A, H58A, and Y29A) resulted in a reduced rate of iron oxidation, with the maximal reduction observed in the case of E22A; however, in none of these cases did the mutation show any influence on the self-assembling property of the protein, indicating a lack of a direct correlation between self-assembly and ferroxidase activity (Figure 5). Mutant E122A present at the lining of the 3-fold channel had no influence on assembly formation but a significant reduction of 30% in ferroxidase activity (Figure 5).

dx.doi.org/10.1021/bi301189t | *Biochemistry* 2013, 52, 1694−1704

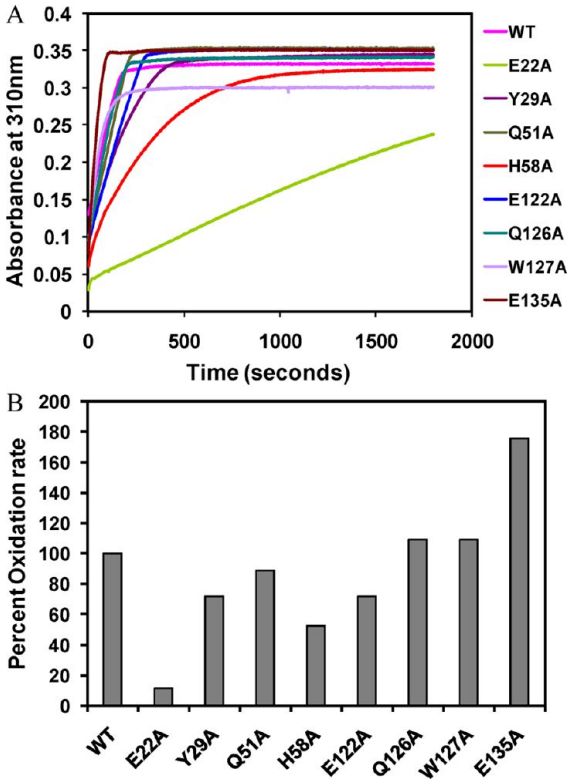

Figure 5. Influence of various mutations on the iron oxidation activity of BfrB. (A) WT BfrB and its mutants (0.25 μM) were mixed with ferrous ammonium sulfate (125 μM) in 0.1 M HEPES (pH 6.5), and iron oxidation was monitored by the increase in absorbance at 310 nm. (B) Bar diagram representation of the percent oxidation rate of WT BfrB and its mutants. Few mutations at the ferroxidase center led to a substantially reduced oxidation rate; however, BfrB E135A showed an increased rate of oxidation. Two separate experiments were conducted, and one of the representative curves is depicted.

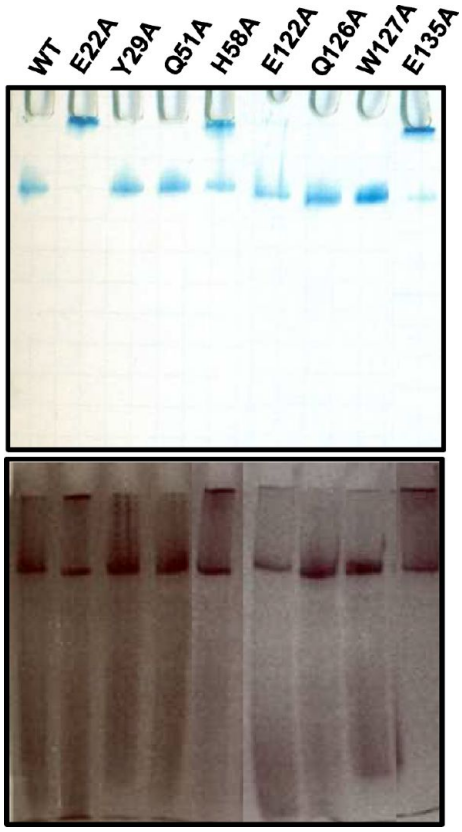

Figure 6. Measurement of iron uptake activity of WT BfrB and its mutants. Ammonium ferrous sulfate (0.5 mM) was mixed with 20 μg of WT BfrB or a mutant in 0.1 M HEPES (pH 6.5) in a reaction volume of 40 μL and incubated for 2 h at room temperature. The samples were then loaded on a 7.5% native polyacrlyamide gel and stained with Coomassie Brilliant Blue for protein staining and Prussian blue for iron staining.

E135A represented a rather unusual class of mutants that exhibited no alteration in the assembly formation despite a markedly reduced level of secondary structure, yet it exhibited an increased thermal stability and a remarkably 80% enhanced ferroxidase activity. The rest of the mutants did not show any significant alteration in their ferroxidase activities (Figure 5).

Influence of Mutations on the Iron Uptake Properties of BfrB. Ferritins store iron molecules inside its cagelike cavity. Uptake studies were performed by incubating the protein with iron molecules in a ratio of 1:500 followed by native gel electrophoresis and subsequently staining the proteins with Prussian blue (Figure 6, top panel) and Coomassie Brilliant Blue (Figure 6, bottom panel). In the case of WT, the protein assembled into a 24-meric form in the absence of iron, and after incubation with iron, the iron molecules were stored within the ferritin shells as marked by the appearance of a distinct blue band on staining with Prussian blue (Figure 6). However, as described below, there could be a few exceptions in which specific mutations could change the property of the protein in a manner such that it may tend to multimerize into much higher-molecular mass aggregates. Among the substitutions at the ferroxidase center, the uptake exhibited by the Y29A mutant was similar to that of wild-type BfrB. Despite the presence of cagelike structures, mutant E22A failed to store iron because of its inability to exhibit ferroxidase activity; hence, it precipitated possibly because of the presence of insoluble Fe(III) resulting from autoxidation (Figure 6). However, mutant H58A showed perfect iron cores as well as iron-induced precipitation. Another class of mutants included Q51A, E122A, Q126A, and W127A, which resulted in the formation of proper holoferritins similar to the wild-type protein. A striking observation was a greatly reduced level of the holoferritin (iron-bound oligomer) in the case of mutant E135A, which precipitated despite its enhanced ferroxidase activity (Figure 6).

DISCUSSION

In this study, bacterioferritin B of *M. tuberculosis* was subjected to mutagenesis to improve our understanding of the protein–protein interactions and to identify crucial residues involved in the formation of its macromolecular assembly and functional properties. On the basis of the analysis of the crystal structure of BfrB, we developed 12 mutants of this nanocage protein of *M. tuberculosis* by employing site-directed mutagenesis (Figure 1). Various residues were selected to identify amino acids mediating surface interactions and thermodynamic stability in addition to residues involved in ferroxidase activity. A highly conserved residue, R69, or its analogous position is involved in the formation of a salt bridge in the proximity of 3-fold channels.[26] Residues E122, Q126, W127, and L129 are present along the 3-fold channels of the protein and are predicted for their possible involvement in the interactions with the neighboring subunits.[26] W127 of BfrB, present near the 3-

dx.doi.org/10.1021/bi301189t | *Biochemistry* 2013, 52, 1694–1704

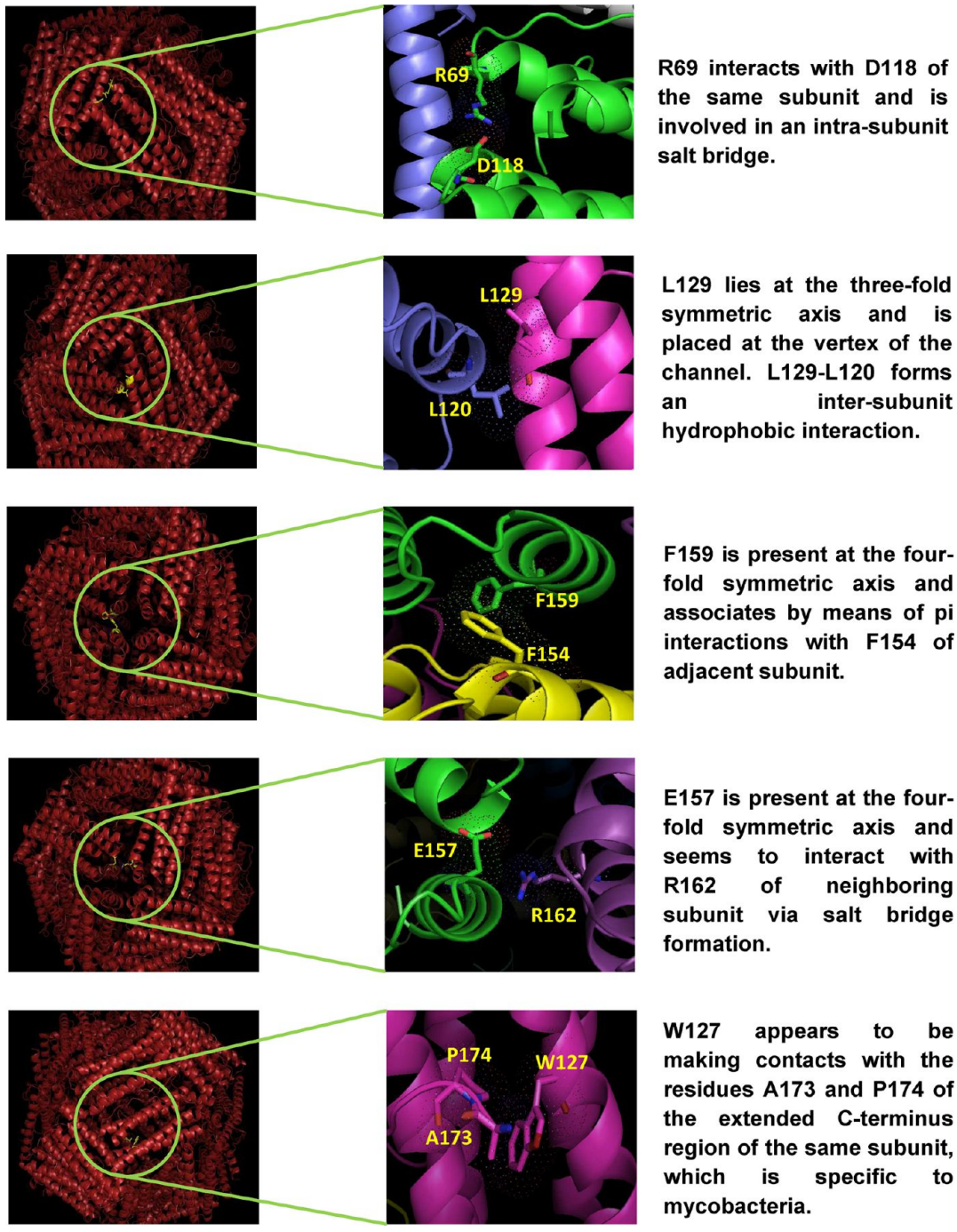

Figure 7. Involvement of switch residues influencing assembly formation in various inter- and intrasubunit interactions. The left panel shows an overall view of the switch residues (yellow inside the circles) involved in subunit interactions. The right panel shows a closer look at the interaction. The figure clearly shows that mutation of all the switch residues is likely to render them unable to form the assembly as these residues are involved in interactions with either the same or the neighboring subunits of the protein.

fold channel, is predicted to be involved in the interactions not present in homologous proteins and is specifically associated with the mycobacterial ferritin interactions.[26] L129 is another important residue that is present at the 3-fold symmetry axis and is predicted to be involved in performing the role of a pore gate in addition to forming an intersubunit hydrophobic contact with adjacent residues.[21,26] F159, which is present in the 4-fold symmetry axis, has been reported by us to be involved in π-electron interactions in mycobacterial BfrB and appears to play a key role in inter- and intrasubunit interactions.[26] E157, present at a 4-fold channel, is another residue associated with salt bridge formation and has been shown to be involved in intersubunit interactions.[26] The ferroxidase center, where catalysis occurs, is known for the presence of conserved residues such as Y29, H58, and E22, whereas Q51 and E135 are associated with the metal binding sites in several ferritins.[16,17] Hence, the residues mentioned above were chosen for mutagenesis.

The size exclusion chromatographic analysis along with the native gel electrophoresis and electron microscopic studies

dx.doi.org/10.1021/bi301189t | *Biochemistry* 2013, 52, 1694−1704

showed that four mutants (R69A, L129P, F159A, and E157A/F159A) existed as subunit dimeric species and failed to form the 24-meric characteristic assembly of ferritins (Figures 2 and 3). The BfrB structure revealed the presence of a salt bridge between residues R69 and D118 (Figure 7), and the inability of the R69A mutant to assemble into a 24-meric structure suggests a crucial role of this salt bridge in the intrasubunit interactions leading to the formation of the assembled protein.[26] The cognate Arg residue has also been substituted in other homologous proteins such as *E. coli* Bfr and frog ferritin.[22,25] Although, in the case of *E.coli* Bfr, the Arg residue involved in the formation of the salt bridge is structurally not equivalent to R69 of *M. tuberculosis* BfrB, its substitution also resulted in the failure of assembly formation. In contrast, however, in the case of frog ferritin, the Arg substitution did not alter its ability to assemble. Residue L129, present at the 3-fold channel, forms an intersubunit hydrophobic contact with residue L120 in the crystal structure of *M. tuberculosis* BfrB[26] (Figure 7). Earlier studies with substitutions of the cognate residues resulted in the formation of properly assembled nanocages with enhanced iron exit properties, indicating that it may not be critical for molecular assembly formation in those cases.[21] However, when the residue at this position in the case of *M. tuberculosis* BfrB (L129) was substituted with proline, it led to the failure of the mutant to assemble into a 24-mer, and the mutant existed only as a subunit dimeric species, substantiating the role of this interaction in mediating intersubunit interactions. Thus, it appears that the function of various homologous positions in ferritins could be at variance based on the strength and types of interactions that govern the folding, stability, and function of these proteins; hence, it may not be wise to predict the function of a residue solely on the basis of sequence−structure comparisons. A few studies have demonstrated the role of helix E present at the C-terminus of human ferritin in influencing the stability of the 24-meric structure through inter- and intrasubunit interactions.[31,32] It has been shown that an extension and alteration of the C-terminus result in an increased level of aggregation of the protein, which is suggested to be responsible for neurodegenerative disorders in which nucleotide insertions occur leading to changes at the C-terminus of the protein.[31] Moreover, the loss of helix E has been shown to cause disruption of 4-fold pores.[32] However, in these studies of human ferritin, the assembly of the 24-mer was unaltered by these changes at the C-terminus.[31,32] In our study of mycobacterial ferritin, mutation of residues F159 and E157, present at the 4-fold axis, resulted in complete abrogation of the molecular assembly of the protein. These observations substantiate the importance of residues at the 4-fold axis in the structural integrity of the protein. F159 associates with F154 from the adjacent subunit by means of π interactions; thus, our observations suggest that this interaction plays an important role in assembly formation (Figure 7). In addition, a salt bridge formed by the interaction between E157 and R162 (neighboring subunit) seems to be important for structural assembly formation (Figure 7). It was previously shown by us that deletion of 14 amino acids from the C-terminus of *M. tuberculosis* BfrB led to a decreased thermal stability of the protein along with a reduction in its ferroxidase activity.[26] Hence, this study emphasizes the importance of 4-fold axis residues in the critical function of the macromolecular assembly and stability of the protein (Figure 7). In addition, the mutation of residue W127, the only tryptophan present in *M. tuberculosis* BfrB, as well as residue E122 to alanine resulted in the decreased stability of the assembled form, implicating both these residues in the stability of the self-assembled form. The crystal structure of *M. tuberculosis* BfrB shows intrasubunit interaction of residue W127 with A173 and P174, which is specific to mycobacterial species[26] (Figure 7). In light of the observed influence of mutating W127 on the thermal stability of the protein, the interaction among these three residues might contribute to the stability of the assembled protein (Figure 7).

Generally, ferritin nanocages are relatively stable proteins. Mutations that lead to a predominance of the subunit dimeric form can provide information not only about the residues involved in molecular assembly but also about their contribution in providing stability to the protein. The mutations of R69, L129, F159, and E157 and F159 resulted in the subunit dimeric forms devoid of the ability to self-assemble into 24-mer units (Figure 2). These subunit dimeric mutants were considerably thermolabile, melting at a low temperature of ∼30 °C (Figure 4C), suggesting that the macromolecular assembly of BfrB enhances the stability of the assembled form; however, the subunit dimeric forms have been isolated in the case of only few ferritins, and the results do not necessarily follow the same principle.[25] In the case of *E. coli* Bfr, the subunit dimeric forms were even more stable than the self-assembled protein; however, in the case of *R. capsulatum*, which like mycobacterium is a Gram-positive organism and evolutionarily more closer to mycobacteria than *E. coli* is, the subunit dimeric forms were very less stable, as observed in the case of mycobacteria.[24,25] Thus, from these limited observations, it may not be prudent to predict any principle for governing the stability of dimers and assembled proteins. The mutations of residues E135, Q51, and Q126 provided very interesting information about the stability of the protein. Although all three mutants were assembled as the wild-type protein, their thermal stability was significantly enhanced, resulting in melting temperatures higher by ∼10−15 °C (Figure 4C). It is fascinating that a single-point mutation can enhance the stability of the protein without affecting its structure or assembly. It is very tempting to use these observations to speculate about the existence of thermodynamic "hot spots" in proteins that have already been proposed by several investigators. We believe that such observations could be remarkably used as a stepping stone in the design of thermostable nanocages by using site-directed mutagenesis.

Ferritins represent macromolecular structures of well-assembled 24-mer subunits and exhibit iron oxidation as well as iron storage properties. As expected, the substitution of ferroxidase site residues E22, Y29, and H58 resulted in a reduced rate of iron oxidation; in fact, the E22A mutation resulted in an ∼90% loss of iron oxidation activity (Figure 5). Some ferritins have two metal binding sites,[33] while others possess three metal binding sites.[13,17,34] The crystal structure of *M. tuberculosis* BfrB evidently has only two metal binding sites, A and B.[26] The third metal binding site, C, is apparently not present as one of the key residues, E54, is flipped in the other orientation.[26] The substitution of residue E135, which is also a constituent of the metal binding C site, resulted in an ∼80% increased iron oxidation rate in comparison to that of the wild-type protein (Figure 5B). Moreover, this mutant exhibited a significantly reduced rate of iron incorporation along with iron-induced aggregation of the mutant protein (Figure 6). It appears that E135 is involved in the movement and translocation of iron; hence, the mutation would lead to immediate leaching of the iron molecules without being stalled

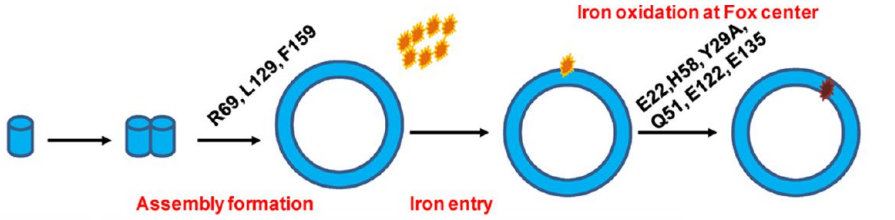

Mutation	Functional role of residue	Mutation	Functional role of residue
E22A	Iron oxidation	Q126A	Three-fold channel
Y29A	Iron oxidation	W127A	Three-fold channel
Q51A	Iron oxidation	L129P (D)	Subunit interaction
H58A	Iron oxidation	E135A	Metal binding site
R69A(D)	Subunit interaction	F159A(D)	Subunit interaction
E122A	Iron oxidation	E157A/F159A (D)	Subunit interaction

Figure 8. Schematic representation describing the influence of various mutations on the assembly formation, iron oxidation, and iron release activity of *M. tuberculosis* BfrB. The model depicts the identification of crucial residues of BfrB involved in assembly formation, subunit interaction, and ferroxidase (Fox) activity. The table shows the plausible role of each residue in the proper functioning of the protein (D denotes the mutants that existed as subunit dimeric forms as a result of disruption of their macromolecular assembly).

by E135, and this immediate clearance in turn would cause more iron oxidation. Moreover, a much enhanced oxidation rate with a dysregulated mode of transfer of iron to the cavity might lead to leaching of the excess oxidized iron into the solution rather than it being stored into the core, leading to the formation of insoluble iron aggregates that would cause precipitation of the mutant protein. This is supported by our uptake studies in which most of the E135A mutant protein underwent aggregation.

In summary, by probing with various techniques, we have identified residues that are structurally, functionally, and energetically important for BfrB, a nanocage protein of *M. tuberculosis*. A schematic model representing the role of the selected residues in molecular assembly and function of this ferritin is shown in Figure 8. Four mutants lacked the ability to assemble into nanocage structure and existed as stable subunit dimers in solution. We also identified three residues that when substituted by alanine imparted enhanced thermal stability to the protein, which could contribute significantly to the development of novel thermoresistant nanocages with enhanced strength. In addition, we also identified residues involved in iron oxidation activity. This study emphasizes that single-point mutations can have the potential to alter multiple properties of the protein. Besides, switch residues or interface hot spots identified in this study could also prove to be extremely helpful for the rational design of interfacial inhibitors.

■ ASSOCIATED CONTENT

Ⓢ Supporting Information

Expression analysis of the *bfrB* gene using polyacrylamide electrophoresis, purification of WT BfrB, evaluation of the iron content of purified WT BfrB and the role of iron in the assembly formation of the protein, effect of changes in pH on the iron autoxidation and protein-mediated oxidation, and iron oxidation curves of BfrB mutants in comparison to those of WT BfrB and control buffer. This material is available free of charge via the Internet at http://pubs.acs.org.

■ AUTHOR INFORMATION

Corresponding Author

*E-mail: aniltyagi@south.du.ac.in. Telephone: 91-11-24110970. Fax: 91-11-24115270.

Funding

This work was supported by a financial grant received from the Department of Biotechnology, Government of India. G.K. and P.N. are grateful to the Council of Scientific and Industrial Research, India, for a fellowship.

Notes

The authors declare no competing financial interest.

■ ACKNOWLEDGMENTS

We acknowledge the Central Instrumentation Facility at UDSC for Circular Dichroism studies and the Advanced Instrumentation Research Facility (AIRF), Jawaharlal Nehru University, Delhi, for TEM studies. Rakesh K. Gupta (Department of Microbiology, Ram Lal Anand College, University of Delhi) and Vibha Gupta are acknowledged for useful discussions. We acknowledge Sandeep Kumar and Priti Singh for excellent technical help and Rajiv Chawla for excellent secretarial help.

■ ABBREVIATIONS

SEC, size exclusion chromatography; TEM, transmission electron microscopy; CD, circular dichroism; Bfr, bacterioferritin.

■ REFERENCES

(1) Arosio, P., and Levi, S. (2002) Ferritin, iron homeostasis, and oxidative damage. *Free Radical Biol. Med. 33*, 457−463.

(2) Theil, E. C. (2003) Ferritin: At the Crossroads of Iron and Oxygen Metabolism. *J. Nutr. 133*, 1549S−1553S.

(3) Andrews, S. C., Robinson, A. K., and Rodríguez-Quiñones, F. (2003) Bacterial iron homeostasis. *FEMS Microbiol. Rev. 27*, 215−237.

(4) Liu, X., and Theil, E. C. (2005) Ferritins: Dynamic management of biological iron and oxygen chemistry. *Acc. Chem. Res. 38*, 167−175.

(5) Smith, J. L. (2004) The physiological role of ferritin-like compounds in bacteria. *Crit. Rev. Microbiol. 30*, 173−185.

(6) Lim, M. K., Lee, C. K., Ju, Y. S., Cho, Y. S., Lee, M. S., Yoo, B., and Moon, H. B. (2001) Serum ferritin as a serologic marker of activity in systemic lupus erythematosus. *Rheumatol. Int. 20*, 89−93.

(7) Zandman-Goddard, G., and Shoenfeld, Y. (2007) Ferritin in autoimmune diseases. *Autoimmun. Rev. 6*, 457−463.
(8) Rodriguez, G. M., Voskuil, M. I., Gold, B., Schoolnik, G. K., and Smith, I. (2002) ideR, an essential gene in *Mycobacterium tuberculosis*: Role of IdeR in iron-dependent gene expression, iron metabolism, and oxidative stress response. *Infect. Immun. 70*, 3371−3381.
(9) Waidner, B., Greiner, S., Odenbreit, S., Kavermann, H., Velayudhan, J., Stahler, F., Guhl, J., Bisse, E., van Vliet, A. H., Andrews, S. C., Kusters, J. G., Kelly, D. J., Haas, R., Kist, M., and Bereswill, S. (2002) Essential role of ferritin Pfr in *Helicobacter pylori* iron metabolism and gastric colonization. *Infect. Immun. 70*, 3923−3929.
(10) Reddy, P. V., Puri, R. V., Khera, A., and Tyagi, A. K. (2012) Iron Storage Proteins Are Essential for the Survival and Pathogenesis of *Mycobacterium tuberculosis* in THP-1 Macrophages and the Guinea Pig Model of Infection. *J. Bacteriol. 194*, 567−575.
(11) Cabán-Hernández, K., Gaudier, J. F., and Espino, A. M. (2012) Characterization and differential expression of a ferritin protein from *Fasciola hepatica*. *Mol. Biochem. Parasitol. 182*, 54−61.
(12) Bevers, L. E., and Theil, E. C. (2011) Maxi- and mini-ferritins: Minerals and protein nanocages. *Prog. Mol. Subcell. Biol. 52*, 29−47.
(13) Stillman, T. J., Hempstead, P. D., Artymiuk, P. J., Andrews, S. C., Hudson, A. J., Treffry, A., Guest, J. R., and Harrison, P. M. (2001) The high-resolution X-ray crystallographic structure of the ferritin (EcFtnA) of *Escherichia coli*; comparison with human H ferritin (HuHF) and the structures of the Fe^{3+} and Zn^{2+} derivatives. *J. Mol. Biol. 307*, 587−603.
(14) Lawson, D. M., Artymiuk, P. J., Yewdall, S. J., Smith, J. M., Livingstone, J. C., Treffry, A., Luzzago, A., Levi, S., Arosio, P., Cesareni, G., Thomas, C. D., Shaw, W. V., and Harrison, P. M. (1991) Solving the structure of human H ferritin by genetically engineering intermolecular crystal contacts. *Nature 349*, 541−544.
(15) Ren, B., Tibbelin, G., Kajino, T., Asami, O., and Ladenstein, R. (2003) The multi-layered structure of Dps with a novel di-nuclear ferroxidase center. *J. Mol. Biol. 329*, 467−477.
(16) Lawson, D. M., Treffry, A., Artymiuk, P. J., Harrison, P. M., Yewdall, S. J., Luzzago, A., Cesareni, G., Levi, S., and Arosio, P. (1989) Identification of the ferroxidase centre in ferritin. *FEBS Lett. 254*, 207−210.
(17) Stillman, T. J., Connolly, P. P., Latimer, C. L., Morland, A. F., Quail, M. A., Andrews, S. C., Treffry, A., Guest, J. R., Artymiuk, P. J., and Harrison, P. M. (2003) Insights into the effects on metal binding of the systematic substitution of five key glutamate ligands in the ferritin of *Escherichia coli*. *J. Biol. Chem. 278*, 26275−26286.
(18) Wade, V. J., Levi, S., Arosio, P., Treffry, A., Harrison, P. M., and Mann, S. (1991) Influence of site-directed modifications on the formation of iron cores in ferritin. *J. Mol. Biol. 221*, 1443−1452.
(19) Treffry, A., Bauminger, E. R., Hechel, D., Hodson, N. W., Nowik, I., Yewdall, S. J., and Harrison, P. M. (1993) Defining the roles of the threefold channels in iron uptake, iron oxidation and iron-core formation inferritin: A study aided by site-directed mutagenesis. *Biochem. J. 15*, 721−728.
(20) Theil, E. C., Takagi, H., Small, G. W., He, L., Tipton, A. R., and Danger, D. (2000) The ferritin iron entry and exit problem. *Inorg. Chim. Acta 297*, 242−251.
(21) Takagi, H., Shi, D., Ha, Y., Allewell, N. M., and Theil, E. C. (1998) Localized unfolding at the junction of three ferritin subunits. A mechanism for iron release? *J. Biol. Chem. 273*, 18685−18688.
(22) Jin, W., Takagi, H., Pancorbo, B., and Theil, E. C. (2001) "Opening" the ferritin pore for iron release by mutation of conserved amino acids at interhelix and loop sites. *Biochemistry 40*, 7525−7532.
(23) Takahashi, T., and Kuyucak, S. (2003) Functional properties of threefold and fourfold channels in ferritin deduced from electrostatic calculations. *Biophys. J. 84*, 2256−2263.
(24) Kilic, M. A., Spiro, S., and Moore, G. R. (2003) Stability of a 24-meric homopolymer: Comparative studies of assembly-defective mutants of *Rhodobacter capsulatus* bacterioferritin and the native protein. *Protein Sci. 12*, 1663−1674.
(25) Zhang, Y., Raudah, S., Teo, H., Teo, G. W., Fan, R., Sun, X., and Orner, B. P. (2010) Alanine-shaving mutagenesis to determine key interfacial residues governing the assembly of a nano-cage maxi-ferritin. *J. Biol. Chem. 285*, 12078−12086.
(26) Khare, G., Gupta, V., Nangpal, P., Gupta, R. K., Sauter, N. K., and Tyagi, A. K. (2011) Ferritin structure from *Mycobacterium tuberculosis*: Comparative study with homologues identifies extended C-terminus involved in ferroxidase activity. *PLoS One 6*, e18570.
(27) Fan, R., Boyle, A. L., Cheong, V. V., Ng, S. L., and Orner, B. P. (2009) A helix swapping study of two protein cages. *Biochemistry 48*, 5623−5630.
(28) Zhang, Y., Fu, J., Chee, S. Y., Ang, E. X., and Orner, B. P. (2011) Rational disruption of the oligomerization of the mini-ferritin *E. coli* DPS through protein-protein interface mutation. *Protein Sci. 11*, 1907−1917.
(29) Stookey, L. L. (1970) Ferrozine: A new spectrophotometric measurement for iron. *Anal. Chem. 42*, 779−781.
(30) Waldo, G. S., and Theil, E. C. (1993) Formation of iron(III)-tyrosinate is the fastest reaction observed in ferritin. *Biochemistry 32*, 13262−13269.
(31) Baraibar, M. A., Barbeito, A. G., Muhoberac, B. B., and Vidal, R. (2008) Iron-mediated aggregation and a localized structural change characterize ferritin from a mutant light chain polypeptide that causes neurodegeneration. *J. Biol. Chem. 283*, 31679−31689.
(32) Baraibar, M. A., Muhoberac, B. B., Garringer, H. J., Hurley, T. D., and Vidal, R. (2010) Unraveling of the E-helices and disruption of 4-fold pores are associated with iron mishandling in a mutant ferritin causing neurodegeneration. *J. Biol. Chem. 285*, 1950−1956.
(33) Toussaint, L., Bertrand, L., Hue, L., Crichton, R. R., and Declercq, J. P. (2007) High-resolution X-ray structures of human apoferritin H-chain mutants correlated with their activity and metal-binding sites. *J. Mol. Biol. 365*, 440−452.
(34) Treffry, A., Zhao, Z., Quail, M. A., Guest, J. R., and Harrison, P. M. (1998) How the presence of three iron binding sites affects the iron storage function of the ferritin (EcFtnA) of *Escherichia coli*. *FEBS Lett. 432*, 213−218.